Flame soot generated under controlled combustion conditions: Heterogeneous reaction of NO2 on hexane soot

ARTICLE *in* INTERNATIONAL JOURNAL OF CHEMICAL KINETICS · NOVEMBER 2002

Impact Factor: 1.52 · DOI: 10.1002/kin.10091

2 AUTHORS:

Sagrario Salgado
University of Castilla-La Mancha
47 PUBLICATIONS **317** CITATIONS
SEE PROFILE

Michel J Rossi
Paul Scherrer Institut
259 PUBLICATIONS **6,494** CITATIONS
SEE PROFILE

Flame Soot Generated Under Controlled Combustion Conditions: Heterogeneous Reaction of NO_2 on Hexane Soot

M. S. SALGADO, M. J. ROSSI

Laboratory of Air and Soil Pollution, Swiss Federal Institute of Technology, CH-1015 Lausanne, Switzerland

Received 25 February 2002; accepted 26 July 2002

DOI 10.1002/kin.10091

ABSTRACT: We used a Combustion Aerosol Standard burner unit that affords controlled and adjustable flame conditions, and adapted it for use with liquid fuel. We prepared samples of hexane soot under different well-defined combustion conditions, and probed the chemical properties of hexane soot by using its heterogeneous interaction with NO_2 in a Knudsen flow reactor. Soot generated under conditions of fuel to oxygen ratio near stoichiometry ($\lambda = 0.82$) produced HONO as the main product. Yields of HONO decreased for soot generated under lean conditions ($\lambda = 0.16$). Finally, NO was the principal product of the reaction for soot generated under extremely lean conditions ($\lambda = 0.09$) corresponding to the lower flammability limit. We may conclude that the combustion conditions determined surface properties gauged by the heterogeneous NO_2–soot interaction. © 2002 Wiley Periodicals, Inc. Int J Chem Kinet 34: 620–631, 2002

INTRODUCTION

When any hydrocarbon fuel is burnt under oxygen-deficient conditions, soot aerosol particles will be produced, which are formed by incomplete combustion of carbonaceous fuels. Loadings of elemental carbon suspended in the atmospheric boundary layer range from 1.5–20 μg m^{-3} (urban areas) to 0.2–2 μg m^{-3} (rural areas) [1]. In the lower troposphere, the principal sources of soot aerosol are fossil fuel and biomass burning [2,3]. In the upper troposphere and lower stratosphere, the primary source of soot is jet aircraft exhaust [4].

The presence of these particles emitted by combustion processes causes several important environmental effects such as respiratory health effects at the high concentrations found in urban environments [3] and scattering and absorption of visible radiation limiting atmospheric visibility. Particulates affect the Earth's climate both directly by scattering and absorbing incoming solar radiation [5] and indirectly by serving as nuclei for cloud formation [6–8]. They also provide active sites for surface and condensed-phase chemistry to take place in the atmosphere. However, soot is not only

Present address of M. S. Salgado: Departamento de Química Física, Facultad de Ciencias, Universidad de Castilla La Mancha, Avda. Camilo José Cela, 10, 13071 Ciudad Real, Spain.

Correspondence to: M. J. Rossi; e-mail: michel.rossi@epfl.ch.

Contract grant sponsor: OFES.

Contract grant sponsor: Universidad de Castilla La Mancha.

an undesired pollutant but also a commercial product such as carbon black or amorphous carbon, which is manufactured on an industrial scale for more than 50 years. It is basically used as a pigment for printing inks and coatings or as an additive in order to improve the mechanical properties, the UV resistance, and the mechanical wear of polymers such as automobile tires.

The reactivity of soot and its potential catalytic activity depend on the nature of the functional groups present on the substrate surface [9]. It is important to mention that its fractal structure offers a large specific surface area for heterogeneous reactions. Many studies have been done in order to identify the chemical functionalities and compounds that are present in soot, both for environmental samples as well as for laboratory-generated soot [10–16].

In view of the importance of soot as a by-product of combustion the heterogeneous reactions of gaseous pollutants such as SO_2, NO_x, HNO_3, and O_3 with soot are of atmospheric importance, both from the point of view of the atmospheric balance of pollutants as well as a potential source for new pollutants. A well-known example is the synergistic interaction of SO_x/NO_x on soot [17] to produce sulphate which has been implied in climate change. Several investigations of the kinetics of ozone loss on soot substrates have been performed [18–22]. O_3 undergoes a chemical oxidation reaction with soot to result in CO and CO_2 as well as some unidentified oxidation products remaining adsorbed on the carbon [18] rather than catalytic decomposition as has been widely believed. The wide range of observed reaction probabilities may be due to differences in experimental techniques, different types of soot substrates or differing extents of soot oxidation, and passivation arising from prolonged exposure to ozone. The heterogeneous reactions of HNO_3 on carbon aerosols have been studied by several research groups who report NO and NO_2 as principal products [22–26], although no important HNO_3 depletion is observed in some of these studies. A number of studies have examined the heterogeneous reactions of NO_2 with the surface of soot particles in view of the fact that NO is unreactive under most experimental conditions. The rate of black carbon oxidation by NO_2 for temperatures above 475 K leads to the formation of NO, CO, and CO_2 [27] in distinct contrast to ambient temperature, which is discussed later. The heterogeneous reaction of NO_2 on soot has also been investigated as a simulated diesel exhaust plume in a dielectric barrier discharge reactor where NO, HONO, and other products have been observed [28].

One of the reaction products of NO_2 with soot substrates is HONO, which is an important trace gas in the atmosphere because it is easily photolyzed to $OH + NO$. Heterogeneous formation of HONO resulting from the reaction of NO_x with absorbed H_2O has been known for a long time through laboratory studies but they do not explain the HONO concentrations in the atmosphere because this reaction is too slow [29]. All known homogeneous gas phase processes have been ruled out to be responsible for the build-up of atmospheric HONO so that the search has focused on the study of heterogeneous reactions as a possible source of HONO [30–43]. However, the detailed mechanism of HONO formation in the atmosphere is not yet fully understood and probably involves several different pathways.

Heterogeneous reactions of NO_2 on soot have been proposed in order to explain discrepancies between field measurements and model calculations [44]. Model calculations that include all known homogeneous gas-phase reactions resulting in HONO underestimate the measured HONO concentration by a factor of 10–100. The calculations with a photochemical box model show that the conversion of NO_2 to HONO on particle surfaces produces a large, measurable signal in nighttime HONO mixing ratios [42]. Recent kinetic investigations indicate that the heterogeneous production of HONO from NO_2 on suspended soot particles proceeds 10^5–10^7 times faster than on previously studied surfaces, and proposed that this interaction may account for the high concentrations of HONO in air masses where combustion sources contribute to air pollution by soot and NO_2 emissions [39,40].

Soot aerosol particles are composed of amorphous carbon and may contain to an extent of up to 50 wt%, an organic fraction [45] that consists of semivolatile hydrocarbons such as polycyclic aromatic and partially oxygenated organic compounds [10,11]. In order to produce soot in the laboratory, several methods are described in the literature: collection of soot in the burnt gases of fuel combustion [22], production of carbonaceous material by using a spark discharge generator equipped with graphite electrodes [25,30], soot resuspension of commercially available soot by using a brush generator [30], or using a diffusion flame [33,38]. These are some of the methods leading to the most reproducible results at present. Regarding the use of diffusion flames, there are a number of unresolved questions such as the strong temporal and spatial variation of the thermal and chemical properties of the diffusion flame (flickering flame), the dependence of the combustion process on the rate of mixing rather than on the rate of the chemical reactions, the rough estimation of the fuel/oxygen ratio, and the continuous adjustment of the air flow during sample collection in order to maintain a steady flame of constant appearance.

For gaseous fuels, a CAST (Combustion Aerosol Standard) generator for the generation of well-defined soot aerosols has been developed by Lianpeng Jing at the Swiss Federal Institute of Metrology. The CAST burner unit affords controlled and adjustable flame conditions with defined metrology of the soot particulates. Its construction and operation allows the generation of suspended particles in a wide size and concentration range with a reproducibility of typically ±5% as far as the size distribution is concerned. The chemical composition and morphology are similar to soot aerosol emitted from combustion processes.

In this work we have used the CAST burner and adjusted it for use with liquid hexane fuel. We have prepared samples of hexane soot from a stable flame of known stoichiometry under different conditions and have probed the chemical properties of the interface of the resulting soot by using NO_2 as a chemical probe. We have also reported on the kinetics of NO_2 uptake on different types of soot generated in the CAST as well as the product yields obtained in a Knudsen flow reactor.

EXPERIMENTAL

In the present study different types of hexane soot have been produced. We have adapted CAST for the combustion of liquid fuels in order to produce soot under controlled conditions. The main characteristics of the sample generation method developed are reproducibility and control of combustion conditions. We have coupled the CAST burner unit, usually used in conjunction with a gaseous fuel, to a setup, which produces liquid fuel vapors. The adapted CAST includes the following elements: A constant flow of N_2, controlled by a mass flowmeter is maintained over liquid hexane at a rate allowing the establishment of the vapor–liquid equilibrium in the vessel, which seems to be a key parameter in the control of the soot generation process. An electronically controlled heating system regulates the temperature of hexane as well as of the transfer line connecting the storage vessel with the inlet of the CAST burner. Several thermocouples located at different points allow us to control the temperature and assure that no condensation of hexane occurs. A check valve is located just before the inlet to the burner and protects the system of the possible return of the flame towards the storage vessel. Figure 1 displays the experimental system of soot generation and Fig. 2 illustrates the CAST burner unit. The connection tube temperature must always be at least 10 K higher than the vapor production zone in order to avoid vapor condensation. As a result, we have a controlled mixed gas flow of N_2/hexane corresponding to the vapor pressure of hexane at the chosen

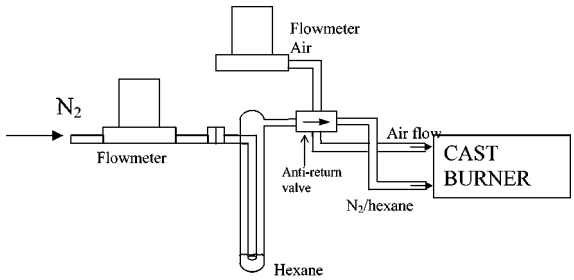

Figure 1 Schematic representation of soot generation system.

temperature. This flow feeds the burner across a fixed point as may be seen in Figs. 1 and 2. The absolute hexane flow has been calculated from the vapor pressure of hexane over its liquid by assuming complete saturation, which we have verified experimentally by measuring, for the three bath temperatures used, the mass of hexane transported during 15 min and compared this quantity with the theoretical mass corresponding to complete saturation. Deviations from complete saturation were distributed on both sides of the 100% value and are always lower than 7%. The air flow necessary for combustion is introduced into the burner across a second port and is controlled by using an additional mass flowmeter. By varying the temperature of the liquid hexane storage vessel, and changing the air flow we may obtain different mixtures of air/hexane. These two parameters have been varied in the present experiments in order to produce soot samples generated at different combustion conditions. When we reduce the temperature and increase the air flow, we obtain leaner conditions. Soot generation conditions are presented in Table I, in terms of the λ value, which is the fuel/oxygen ratio normalized on a per C basis to the stoichiometric value of oxygen, corresponding to the reaction:

$$nC_6H_{14} + 9.5O_2 \rightarrow 6CO_2 + 7H_2O \qquad (1)$$

The vapor pressure of hexane at room temperature is 148.5 Torr. For calculation to other temperatures we

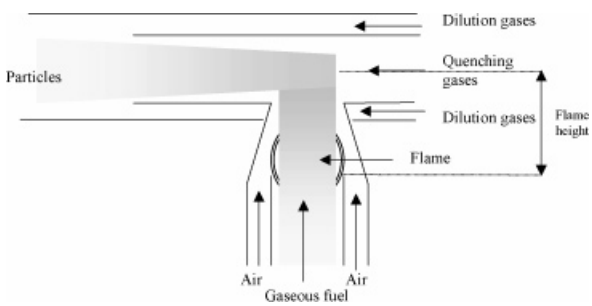

Figure 2 CAST burner unit.

Table I Combustion Conditions During Soot Generation by Using CAST Burner Unit

	Flow rate	Normalization	λ = Fuel/Oxygen	Fuel concentrations (v/v)
Near-stoichiometric conditions				
$F(\text{air}) = 1.35\ \text{l min}^{-1}$	$F(\text{oxygen}) = 270\ \text{ml min}^{-1}$	270/9.5 = 28.42	0.82	$(10.1 \pm 2)\%$
$F(N_2) = 40\ \text{ml min}^{-1}$	$F(\text{fuel}) = 140\ \text{ml min}^{-1}$	140/6 = 23.33		
Lean flame conditions				
$F(\text{air}) = 1.55\ \text{l min}^{-1}$	$F(\text{oxygen}) = 300\ \text{ml min}^{-1}$	300/9.5 = 31.58	0.16	$(2.5 \pm 0.2)\%$
$F(N_2) = 40\ \text{ml min}^{-1}$	$F(\text{fuel}) = 30\ \text{ml min}^{-1}$	30/6 = 5		
Extremely lean flame conditions				
$F(\text{air}) = 1.62\ \text{l min}^{-1}$	$F(\text{oxygen}) = 340\ \text{ml min}^{-1}$	340/9.5 = 35.79	0.09	$(1.15 \pm 0.1)\%$
$F(N_2) = 28\ \text{ml min}^{-1}$	$F(\text{fuel}) = 19\ \text{ml min}^{-1}$	19/6 = 3.17		

may use the equation:

$$\log P = \frac{-0.05332\,a}{T} + b \qquad (2)$$

where P is the pressure in Torr, $a = 31679$, $b = 7.724$, and T is the absolute temperature in K [46].

From now on, soot samples will be referred to as:

(a) soot generated under combustion conditions near stoichiometry ($\lambda = 0.82$),
(b) soot generated under lean fuel conditions ($\lambda = 0.16$),
(c) soot generated under extremely lean fuel conditions ($\lambda = 0.09$). In this case, the flow of N_2 has been reduced to assure saturation of hexane vapor in the carrier gas.

As we may see in Fig. 2 a stream of air concentrically surrounds the gaseous fuel stream. In order to produce soot particles, the symmetrical diffusion flame extends into a cone of steel. A setting of the truncated cone is found whereby the smoke column exits across the top opening of the combustion chamber despite the burning flame. At a certain flame height, the air supply is insufficient for further oxidation of the generated soot particles. The flame heights relative to the cone for the different experiments were 4.3 cm for rich flame conditions (point a) and 3.6 cm for the other two conditions used (points b and c) (Fig. 2).

Leaving the combustion chamber, the particles are wrapped by exhaust gases which develop around the flame and which prevent the particle stream from depositing at the burner walls. N_2 is supplied to the particle stream across the pipe arranged at right angle to the flame axis in order to quench further combustion processes and stabilize the soot particles by dilution. The cold quenching gas inhibits condensation of combustion particles when they escape from the flame unit at ambient air conditions because of a dilution effect. The size distribution and mean diameter of the soot particles generated in the flame unit may be controlled to some extent by judiciously choosing the flows of the different input gases.

NO_2 used for the experiments (Carbagas) is diluted in oxygen (1:10) and stocked in darkness for approximately 14 h in order to convert traces of NO into NO_2 that are always present as a contaminant. Subsequently, NO_2 is frozen out at approximately -80°C in a darkened vessel and the O_2 pumped off.

The kinetic measurements in this work are based on a Knudsen cell, a low pressure flow reactor that operates under molecular flow conditions, using modulated molecular beam mass spectrometry for the quantification of reactant uptake and product release into the gas phase.

Design and operation of the Knudsen cell have been described in detail previously [47] and only a brief description is given here. The apparatus consists of a vacuum line from which molecules are introduced into the two-chamber Knudsen reactor where the interaction of the gaseous species with the substrate of interest takes place and which is connected to the vacuum chamber wherein the mass spectrometer is mounted.

The vacuum line is used to produce, store, and mix gaseous reactants. The gas is continuously injected into the reactor via a glass capillary inlet. The residence time of the gas in the reactor is controlled by means of a variable size orifice through which molecules escape into the vacuum chamber. By changing the orifice size one affects the molecular rate of effusion out of the reactor and may thus vary the molecular residence time (τ) by more than two orders of magnitude. Molecules escape from the reactor forming an effusive (thermal) molecular beam and are detected by an electron impact quadrupole mass spectrometer (QMS) lodged in the lower part of a differentially pumped vacuum chamber. Details of the Knudsen cell are summarized in Table II.

Table II Measured Parameters of the Knudsen Cell Used in this Work[a,b]

Orifice diameter (mm)	k_{esc} (s^{-1})	Residence time (s)	k_{esc} NO_2, 300 K[c] (s^{-1})
1	$0.013 \times (T/M)^{0.5}$	$76.5 \times (M/T)^{0.5}$	0.034
4	$0.245 \times (T/M)^{0.5}$	$4.04 \times (M/T)^{0.5}$	0.441
8	$0.796 \times (T/M)^{0.5}$	$1.23 \times (M/T)^{0.5}$	1.280
14	$1.880 \times (T/M)^{0.5}$	$0.528 \times (M/T)^{0.5}$	4.021

[a] Volume = 2000 cm^3. The total volume is increased by 1% upon opening the sample chamber. Therefore, no distinction concerning the volume is made between a reference and an uptake experiment.

[b] Surface area = 1300 cm^2. Estimated total surface area of the Knudsen Cell. The sample surface area is 19.6 cm^2.

[c] Experimental values obtained by abruptly halting flow.

Each sample has been pumped for 5 min prior to the uptake experiment, and subsequently isolated from the flow, using an O-ring sealed movable plunger. The geometric surface area of the sample chamber is 19.6 cm^2. A new soot sample is used for every uptake experiment and NO_2 is introduced into the cell as a continuous flow (steady-state experiment). NO_2 flows were in the range of 1.49×10^{15}–1.17×10^{16} molecule s^{-1}. When the flow did stabilize, the isolation plunger is lifted and the reaction is monitored. As may be seen in Fig. 3, a large instantaneous rate of NO_2 uptake is observed and quickly saturates within a few minutes. At the same time, we observe product formation. We were able to distinguish different reactivities for the different types of soot tested. The fuel/oxygen ratio is therefore a key parameter influencing the reactivity of soot towards NO_2. The products obtained are different depending on the conditions of soot generation, as is reported later.

RESULTS AND DISCUSSION

We obtained reproducible results for the rate of NO_2 uptake for distinctly different types of soot and have expressed the NO_2 uptake kinetics in terms of a first order uptake coefficient.

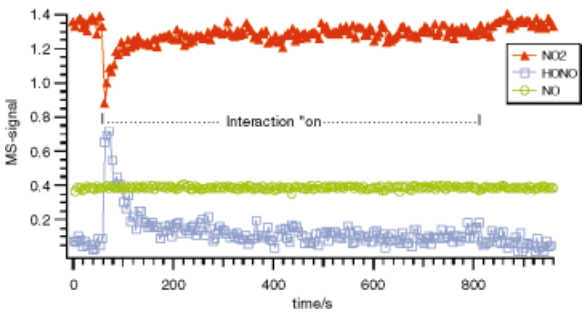

Figure 3 Typical uptake of NO_2 and product formation on soot generated under rich fuel conditions. $[NO_2] = 3.6 \times 10^{11}$ molecule cm^{-3}, soot mass = 8.6 mg, $k_{esc} = 6$ s^{-1} (14-mm diameter escape orifice).

NO_2 Interaction with Hexane Soot Produced Under Near Stoichiometric Combustion Conditions ($\lambda = 0.82$)

The interaction of NO_2 and hexane soot samples originating under conditions near stoichiometry was examined in a series of steady-state experiments by exposing the prepared soot to a continuous flow of NO_2. Figure 3 shows the results of a typical uptake experiment. When the sample is exposed to the NO_2 flow at $t = 60$ s, a large and instantaneous rate of NO_2 uptake (m/e 46) is observed. However, saturation of the soot sample occurs quickly and after a few minutes of interaction the signal attains 85% of its initial value. When the sample chamber is closed at $t = 810$ s, the signal of NO_2 at m/e 46 increases, to reach its original value. Simultaneously to the uptake of NO_2, a large product peak of HONO at m/e 47 appears, which shows that the conversion of NO_2 into HONO is a fast process. The fast decrease of the NO_2 uptake correlates with the large initial rate of HONO formation, which is still observable even at long interaction time. No measurable amounts of NO are produced. The observed HONO yield, defined as the ratio of the amount of HONO released to the amount of NO_2 taken up during the same time, varies between 80 and 50% with the lower value obtained at the higher NO_2 concentrations as displayed in Fig. 4. HONO yields in excess of 50% unambiguously exclude the classical surface catalyzed disproportionation of NO_2 as the dominant process for HONO generation according to reaction (3), which would obtain a HONO yield of 50% at most

$$2NO_2 + H_2O \rightarrow HONO + HNO_3 \qquad (3)$$

We tried to detect HNO_3 at m/e 63 but failed. The yields that significantly exceed the 50% mark and the absence of detectable HNO_3 led us to propose a

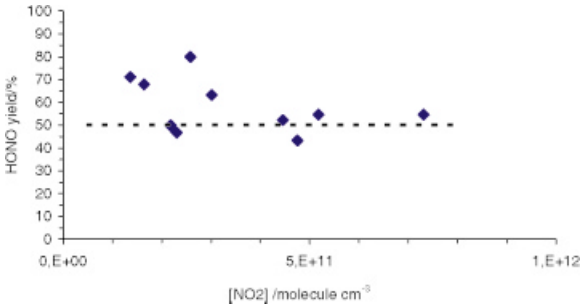

Figure 4 HONO yield relative to NO_2 taken up on soot obtained at conditions near stoichiometry ($\lambda = 0.82$) as a function of [NO_2]. Yields are calculated for 13 min of interaction. Mean sample mass $= 8 \pm 0.8$ mg, 14-mm diameter escape orifice ($k_{esc} = 6\,s^{-1}$), [NO_2] ranges from 1.36×10^{11} to 7.31×10^{11} molecule cm^{-3}. The dashed line indicates the maximum HONO yield of 50% for the disproportionation process, reaction (3).

mechanism which assumes that reducing surface sites on the soot substrate convert NO_2 into HONO following a reduction–oxidation reaction, reactions (4) and (5)

$$NO_2 \rightarrow \{NO_2\} \quad (4)$$

$$\{NO_2\} \text{ or } NO_2 + \{C{-}H\}_{red} \rightarrow HONO + \{C\}_{ox} \quad (5)$$

The species listed in curved brackets refer to surface adsorbates. $\{C{-}H\}_{red}$ represents a surface site that reduces NO_2 to HONO. The interaction of NO_2 with an adsorption site in reaction (4) must be weak, otherwise NO_2 would not be sufficiently mobile to subsequently encounter other surface sites for reaction (5). This reaction must be in competition with a reaction describing the irreversible uptake of NO_2 according to reaction (6):

$$NO_2 + \{S\} \rightarrow \{S{-}NO_2\} \quad (6)$$

This reaction accounts for NO_2, which is absorbed but does not result in an observable gas phase product following the data from Fig. 4. In the present study NO_2 remaining adsorbed on the soot substrate has not been determined. In the past, reaction (3) occurring in the presence of adsorbed H_2O has been invoked as the primary source of heterogeneously formed HONO [25,35,36]. However, it has been shown that the heterogeneous disproportionation of NO_2 in reaction (3) cannot compete against the reduction–oxidation reaction of NO_2 on soot, reaction (5), which most probably is the rate-limiting step for the reduction–oxidation reaction because the latter was orders of magnitude faster than reaction (3) [39,40]. This holds at least in the beginning phases of reaction (5). However, it is possible that it will considerably slow down with progressing evolution of HONO, which may render reaction (3) more competitive, especially on hygroscopic atmospheric particles whose surrogates were examined by Barnes and Finlayson-Pitts in relation to the rate of reaction (3) [36].

In order to estimate the extent of the interaction in terms of its depth into the soot sample as a function of time, a series of NO_2 uptake experiments as a function of the mass of soot were performed. Figure 5 represents the yield of NO_2 taken up and HONO formed in terms of molecules per mg integrated over 13 min as a function of the [NO_2] used in the experiments. The limiting HONO yield over the above integration period is 6×10^{16} molecules of HONO per mg of soot and is a factor of 4 larger than on ethylene soot [40].

Figure 6 displays the uptake of NO_2 as a function of mass of the soot substrate for the 14-mm diameter escape orifice integrated over 1 and 13 min. A good linear dependence of the data as a function of sample mass may be seen along with saturation of the yield of NO_2 taken up and of HONO formed that becomes apparent at a sample mass in excess of 8 ± 2 mg. We conclude that there is no sample mass dependence of the NO_2 loss and HONO yield for the system NO_2-soot beyond the mass of 8 ± 2 mg, which apparently is the minimum mass required to provide a coherent soot coating. This specific soot loading of $(8 \pm 2)/19.6 = 0.41 \pm 0.10$ mg/cm^2 is independent both of the type of soot (see later) and of the integration time within the time scale of the present experiment. In addition, the value for the threshhold loading of 0.41 ± 0.1 mg/cm^2 has been confirmed in earlier work [30,33,34,40]. We further conclude that only the uppermost 8 mg of the soot sample are probed by NO_2 during its gas phase residence time of 0.17 s for the 14-mm escape orifice. Therefore, we divided by 8 the amount of NO_2 taken

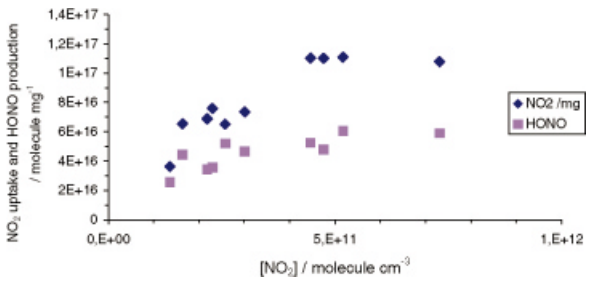

Figure 5 Mass specific NO_2 uptake on soot obtained under combustion conditions near stoichiometry ($\lambda = 0.82$) as a function of [NO_2], 14-mm diameter escape orifice, integrated over 13 min, mean sample mass is 8 ± 0.8 mg.

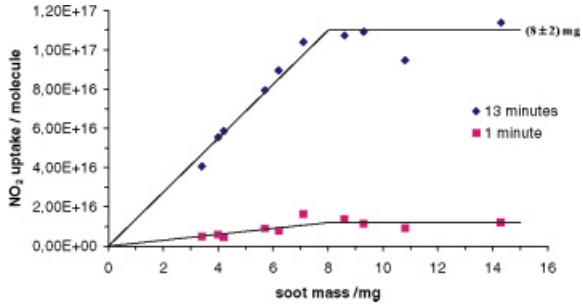

Figure 6 Mass dependence of the NO_2 uptake on soot produced under conditions near stoichiometry ($\lambda = 0.82$). Yields are integrated for 1 and 13 min in the 14-mm diameter orifice reactor and at a mean $[NO_2]$ of 3.6×10^{11} molecule cm^3.

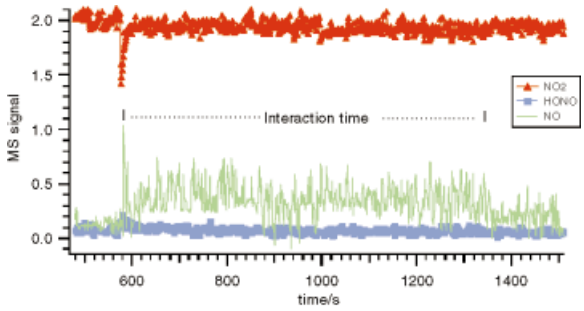

Figure 7 Typical uptake of NO_2 and release of products on soot generated under extremely lean fuel conditions ($\lambda = 0.09$). $[NO_2]$ is 2.24×10^{11} molecule cm^{-3}, soot mass is 7.3 mg spread out over 19.6 cm^2, interaction time is of 13 min.

up in order to present the results on a per mg basis, as displayed in Fig. 6. We thus see no need to apply the pore diffusion theory to the present case in order to correct the yields and uptake kinetics for the effect of pore diffusion of NO_2 within the soot sample [48]. In summary, the soot sample forms a coherent coating once its specific mass exceeds the above-mentioned threshold value in order to form the first sample layer in terms of the pore diffusion theory.

NO_2 Interaction with Hexane Soot Produced in an Extremely Lean Fuel/Oxygen Ratio ($\lambda = 0.09$).

A second series of experiments were performed using hexane soot samples prepared under the most extreme conditions of lean combustion possible for production of soot under our present experimental conditions. This air/fuel mixture coincided with the lower flammability limit of hexane vapor in air whose volume concentration is given in Table I [49]. In these experiments again an instantaneous large uptake of NO_2 with a fast consecutive saturation of the soot sample may be observed. A negligibly small rate of HONO formation is observable essentially during the first few seconds of the reaction. On the other hand, NO monitored at $m/e = 30$ after correction for NO_2 is observed to rise slowly at the beginning to reach a constant value later on. Soot generation in this case is unstable, which may be explained by the fact that the flame was burning at the raw edge of its stability limit [49] and the experimental difficulties do not allow us to systematically study this case. A typical uptake experiment is represented in Fig. 7. The results of the HONO/soot experiments previously performed in our laboratory [33] suggest that NO_2 interacts with black decane soot resulting in the formation of HONO, which to a large extent decomposes by disproportionation into NO and a N(IV) fragment that remains on the soot surface. Therefore, we may assume that HONO is produced initially in the same process that occurs with soot produced under near stoichiometric flame conditions. However, the initially formed HONO decomposes on the soot substrate both to NO that is released into the gas phase and detected, as well as to NO_2, that remains on the surface or undergoes additional reactions with soot. Apparently, only HONO formed in the uppermost soot layers is observed whereas HONO formed in deeper layers is either adsorbed or decomposes to NO, most probably through the decomposition of N_2O_3 according to reaction (7):

$$2\{HONO\} \rightarrow NO + \{NO_2\} + \{H_2O\} \qquad (7)$$

These results are similar to the ones discussed in the literature [33] for the interaction between NO_2 and black soot generated in a diffusion flame.

NO_2 Interaction with Hexane Soot Produced in a Lean Flame ($\lambda = 0.16$)

In these experiments, again an instantaneous large uptake of NO_2 with a fast consecutive saturation of the soot sample may be observed. HONO is the principal product, but yields obtained in this case are smaller than for the case discussed when $\lambda = 0.82$, namely 30% on average, as may be seen in Fig. 8. Figure 9 shows a typical NO_2 uptake experiment performed on soot obtained from lean combustion conditions at $\lambda = 0.16$. The saturation of the loss of NO_2 taken up occurs for soot sample masses larger than 11 ± 2 mg, which is comparable to the results obtained on near-stoichiometric soot of $\lambda = 0.82$ (Fig. 6).

It has been shown in the literature that the reactivity of soot particles towards NO_2 depended on the combustion conditions as far as HONO formation was concerned [37]. Soot aerosol was produced using a

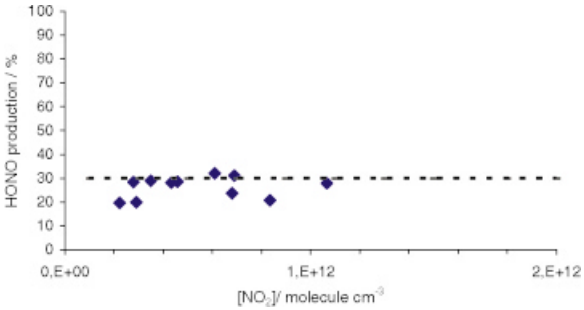

Figure 8 HONO yield relative to NO_2 taken up on soot generated under lean fuel conditions ($\lambda = 0.16$) as a function of [NO_2]. Yields are calculated for 13 min of interaction. Mean sample mass is 11 ± 0.8 mg spread out over 19.6 cm^2, concentration range is $(2.22–10.7) \times 10^{11}$ molecule cm^{-3}. The escape orifice diameter is 14-mm ($k_{esc} = 6\ s^{-1}$). The dashed line indicates the maximum level obtained, that is approximately 30%.

Diesel engine by operating it either under full load or idling conditions. The result was that the HONO formation rate upon interaction of NO_2 with soot generated under full load conditions was higher by a factor of two compared to idling conditions.

Uptake Kinetics of NO_2 on Different Types of Soot

Raw data on the NO_2 interaction with hexane soot generated using the CAST burner show that the rate of uptake strongly decreases during the course of an experiment, as can be seen in Figs. 3, 7, and 9. After an initial fast uptake of NO_2, partial saturation quickly follows. Thus, it is obvious that the uptake probability γ strongly depends on the number of collisions with NO_2 that the sample has experienced. Table III displays the values of γ_0 and γ_{ss} obtained in the NO_2 uptake

Table III γ_0 and γ_{ss} for NO_2 Uptake Experiments on Soot Produced in a Lean Flame ($\lambda = 0.16$) and Near-Stoichiometric Conditions ($\lambda = 0.82$)

[NO_2]/ 10^{11} molecule cm^3	$\gamma_0/10^{-3}$	$\gamma_{ss}/10^{-4}$
Soot generated at $\lambda = 0.16$ (lean)		
4.58	2.88	1.11
4.34	1.19	0.295
2.22	1.72	0.47
2.90	1.25	0.479
2.79	2.06	1.38
3.49	2.40	0.727
10.7	0.76	0.323
8.35	1.46	0.757
5.33	1.985	0.7066
6.06	2.02	0.641
6.89	1.8	0.901
6.80	1.67	0.305
Soot generated at $\lambda = 0.82$ (near stoichiometric)		
5.18	0.8623	1.377
3.59	1.39	1.76
7.31	0.264	0.844
5.62	0.3369	0.497
3.01	1.092	1.666
2.58	0.9696	0.176
4.75	0.754	0.707
5.19	0.7709	0.322
2.30	1.337	0.208
1.36	1.077	1.41
2.18	1.006	0.727
1.64	1.931	0.721

experiments on soot generated at near stoichiometric conditions ($\lambda = 0.82$) and under lean flame conditions ($\lambda = 0.16$).

In Figs. 10 and 11 initial uptake coefficients γ_0 have been calculated and presented as a function of NO_2 concentration for experiments by using fresh hexane

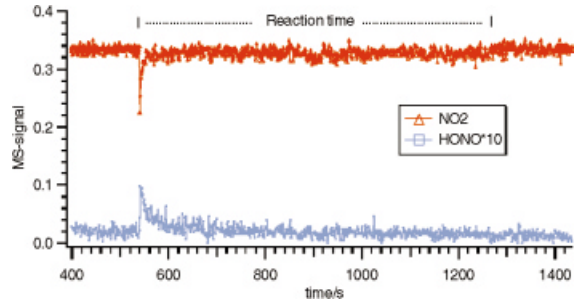

Figure 9 Typical uptake of NO_2 and HONO production on soot generated under lean fuel conditions ($\lambda = 0.16$). [NO_2] is 2.79×10^{11} molecule cm^{-3}, 14-mm diameter escape orifice, mean sample weight is 11 mg spread out over 19.6 cm^2.

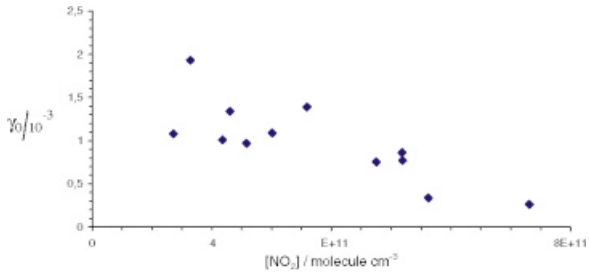

Figure 10 Initial uptake coefficient (γ_0) of NO_2 on soot obtained under combustion conditions near stoichiometry ($\lambda = 0.82$) as a function of [NO_2] in the 14-mm diameter escape orifice. Mean sample weight is 8 ± 0.8 mg spread out over 19.6 cm^2, γ_0 has been calculated using the geometric surface area of the sample.

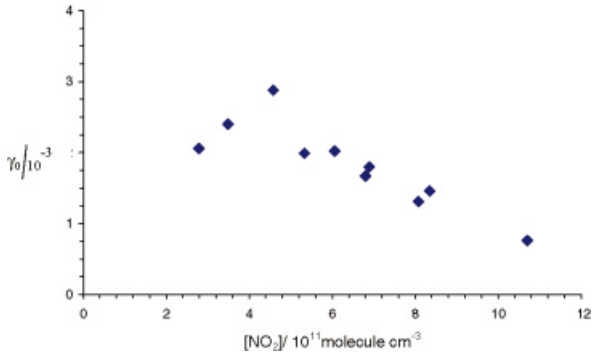

Figure 11 Initial uptake coefficient (γ_0) of NO_2 on soot produced in a lean hexane flame ($\lambda = 0.16$), as a function of $[NO_2]$ in the 14-mm diameter escape orifice reactor. Mean sample weight is 11 ± 0.8 mg, γ_0 has been calculated using the geometric surface area of the sample (19.6 cm^2).

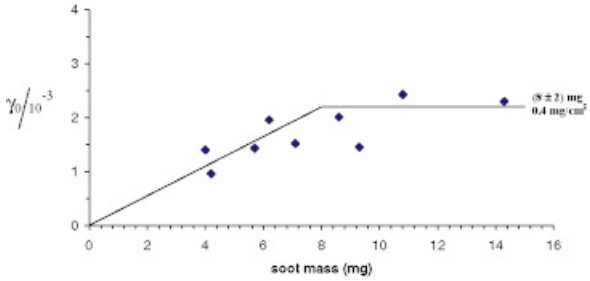

Figure 12 γ_0 vs. soot mass for soot generated under conditions near stoichiometry ($\lambda = 0.82$) in the 14-mm diameter escape orifice at a mean $[NO_2]$ of 3.6×10^{11} molecule cm^3.

soot samples generated near stoichiometric ($\lambda = 0.82$) and lean conditions ($\lambda = 0.16$), respectively. Values of γ_0 are larger by approximately a factor of three for soot obtained at $\lambda = 0.16$ compared to $\lambda = 0.82$ at comparable NO_2 concentration and have been calculated in relation to the geometric surface area of the samples (19.6 cm^2) as the initial uptake coefficients are in any case not subject to correction for pore diffusion. It may be seen that γ_0 continuously decreases with increasing $[NO_2]$. Owing to this fact the kinetics of NO_2 on soot may therefore not be described by a pseudo-first-order rate law. Similarly, γ_{ss} values in Table III reflect the progressing saturation of the samples with increasing $[NO_2]$. Partial saturation of the NO_2 rate of uptake is observed with increasing NO_2 concentration for γ_{ss} as well, which means that the kinetic rate law is more complex than first order. The values of γ_{ss} are one order of magnitude lower compared to γ_0 reflecting the progressive saturation of the sample with reaction time. The steady state uptake coefficients γ_{ss} are in the range of $(0.2–1.7) \times 10^{-4}$ and of the same order for the two types of soot ($\lambda = 0.82$ and $\lambda = 0.16$). The dependence of γ_0 on the mass of the soot sample under conditions near stoichiometry ($\lambda = 0.82$) is presented in Fig. 12. We conclude that there is no significant variation of γ_0 once we have a coherent film of soot, that is for loadings in excess of the limiting value of 8 ± 2 mg in analogy to the results on the mass dependence of NO_2 uptake displayed in Fig. 6. Thereafter, we observe a constant value of γ_0 for any soot mass exceeding this value, leading to a value of γ_0 in the range $(1.5–2.3) \times 10^{-3}$.

Soot Characterization

This study represents a laboratory study that highlights the influence of the combustion conditions on the properties of soot as far as heterogeneous reactivity is concerned. This dependence on the combustion conditions begs the question as to the relevance of the present results to atmospheric combustion aerosol. However, as long as exact information about the nature and type of atmospheric combustion aerosol is lacking one is unable to gauge its heterogeneous reactivity based on the present results. In other words, the information on the makeup and nature of environmental aerosol will have to come from field observations in the future.

The identity of the products of the soot/NO_2 interaction that remain on the sample surface has not been detected in this work. However, in other studies using FTIR absorption spectroscopy and ion chromatography [25,38], absorption bands attributable to surface functional groups such as ─C═O, R─NO_2, R─ONO, and R─ONO_2 have been observed as well as changes in the IR absorption band intensity corresponding to a C─H stretch upon progress of reaction. These results are in good agreement with the reaction mechanism that we propose here. NO_2 reacts on the soot surface and is being reduced thereby leaving the soot surface in a more oxidized state. In addition, NO_2 is in part also irreversibly adsorbed on the soot surface thus becoming stable towards molecular desorption.

Soot samples were examined using elemental analysis in order to obtain more information about their properties. A Carlo Erba EA 1110 Elemental Analyzer was used. Elemental analyzers operate based on a flash combustion in which a sample contained within a tin or silver capsule is dropped into a combustion/reduction reactor (for CHN analyzer) held at 1020°C. The resulting oxidation raises the temperature in excess of 1700°C. The encapsulated sample, depending on its composition, will oxidize generating one or more of these gases: N_xO_x, CO_2, H_2O. Depending on the type of gases one wants to analyze, a combustion/reduction column or separate combustion and reduction columns (usually at 650°C) must be installed in the elemental analyzer furnace. Oxygen can be quantified indirectly

Table IV Elemental Analysis for the Three Types of Soot Generated in this Work in Comparison with Soot Samples from other Studies

	Elemental analysis				
Soot (λ)	C (wt%)	H (wt%)	N (wt%)	O (wt%)	Ref.
$\lambda = 0.82$	94.73 ± 0.15	1.50 ± 0.01	~0	3.78 ± 0.16	This work
$\lambda = 0.16$	93.01 ± 0.31	0.77 ± 0.03	0.26 ± 0.02	7.27 ± 0.42	
$\lambda = 0.09$	92.03 ± 0.34	0.44 ± 0.07	0.23 ± 0.02	5.99 ± 0.36	
Grey decane soot (Rich conditions)	97.27 ± 0.05	0.83 ± 0.04	0.20 ± 0.18	1.65 ± 0.19	[33]
Black decane soot (lean conditions)	96.39 ± 0.22	0.19 ± 0.01	0.27 ± 0.09	3.22 ± 0.25	
n-hexane	87–92.5	1.2–1.6	–	6–11	[10,11]

using a mass balance argument as the combustion takes place in an environment containing an excess of oxygen. This is only valid if other elements such as S or P are present in negligible amounts. Control measurements of acetanilide have regularly been performed in between the analysis of the soot samples. Table IV presents a survey of these results compared to results on soot studied elsewhere [10,11,33]. The table clearly reveals that the composition of the soot for a given fuel depends on the combustion conditions. The oxidative conditions in samples prepared under lean combustion ($\lambda = 0.16$ and $\lambda = 0.09$) are reflected in the higher oxygen content compared to the sample with $\lambda = 0.82$. The opposite trend is observed if the hydrogen contents are examined. In this case the leaner flame shows lower values of the hydrogen content. We assume, as other authors [33] have, that the amount of water adsorbed on soot samples obtained for lean combustion conditions ($\lambda = 0.09$) should be higher compared to soot obtained in a rich flame because its surface should be more polar owing to the higher oxygen content. Soot produced near stoichiometric conditions ($\lambda = 0.82$) has a higher hydrogen content compared to its lean counterparts as expected. We therefore believe that the hydrogen reflects the presence of organic hydrogen for both types of samples.

We have measured the particle size distributions of the soot produced at $\lambda = 0.82$ and $\lambda = 0.16$, using a TSI Scanning Particle Sizer equipped with an impactor in order to remove large particles. In Fig. 13 we observe important differences in both the diameter as well as the width of the distribution between both types of soot (rich and lean flame) leading to an important difference in the mass (volume) concentration between the two different soot samples. The samples have been diluted with 20 l/min of air before analysis.

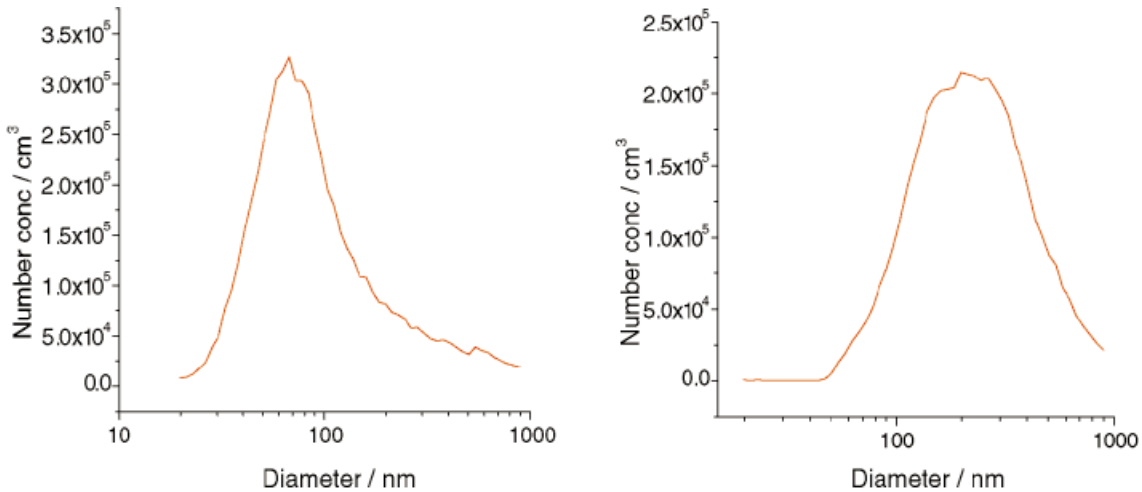

Figure 13 Particle size distribution for soot aerosol produced at combustion conditions near stoichiometry ($\lambda = 0.82$) and at lean conditions ($\lambda = 0.16$), respectively. Mode diameter is 62 nm for the left graph ($\lambda = 0.82$) and 198 nm for the right graph ($\lambda = 0.16$).

CONCLUSIONS

We have adapted an existing diffusion flame burner unit (CAST) to combustion of liquid fuels and probed the different types of soot substrates prepared using NO_2 under molecular flow conditions. Whereas soot produced near stoichiometric conditions ($\lambda = 0.82$) leads to HONO with yields higher than 50% upon interaction with NO_2, smaller yields of HONO of approximately 30% are formed in the presence of soot generated under fuel-lean conditions ($\lambda = 0.16$). We have decreased the fuel/oxygen ratio and have obtained in this case vanishingly small quantities of HONO but important yields of NO. These results are comparable to the ones obtained in the literature [33] for the interaction between NO_2 and black soot, generated in a diffusion flame.

We propose a reaction mechanism in which NO_2 is initially converted to HONO by a reduction–oxidation reaction, which is subsequently quantitatively desorbed into the gas phase on hexane soot generated at $\lambda = 0.82$. Surface functionalities of soot must change with the combustion conditions and NO_2 uptake probabilities and HONO rates of formation are lower if we decrease the fuel/oxygen ratio progressively going to leaner combustion. However, HONO undergoes decomposition on the surface of the soot produced at extremely lean fuel conditions ($\lambda = 0.09$) producing NO, which is instantaneously desorbed into the gas phase, and NO_2, which undergoes secondary reactions on the soot substrate and is therefore not observed.

Uptake coefficients γ decrease rapidly with increasing uptake of NO_2, resulting in steady state values in the range $(0.2–1.7) \times 10^{-4}$.

In conclusion we may affirm that the present set up using the CAST burner unit allows sample soot generation with a high reproducibility and flame stability. Most importantly, the combustion conditions may be varied over a large extent, obtaining soot of different reactivities towards NO_2 and most probably also towards other pollutants.

M. S. Salgado gratefully acknowledges a postdoctoral fellowship obtained from the Spanish Ministry of Education, Culture, and Sports. The help of Prof. A. Merbach and Dr. E. Solari in performing the elemental analysis is very much appreciated. We thank Dr. Lianpeng Jing (Jing-CAST Technology) for the loan of the CAST burner.

BIBLIOGRAPHY

1. Seinfeld, J. H.; Pandis, S. N. Atmospheric Chemistry and Physics: From air pollution to climate change; Wiley: New York, 1998.
2. Penner, J. E.; Novakov, T. J Geophys Res 1996, 101, 19373–19378.
3. Cooke, W. F.; Wilson, J. N. J Geophys Res 1996, 101, 19395–19409.
4. Schumann, U.; Strom, J.; Busen, R.; Baumann, R.; Gierens, K.; Krautstrunk, M.; Schröder, F. P.; Stingl, J. J Geophys Res 1996, 101, 6853–6869.
5. Intergovernmental Panel on Climate Change (ICPP). In Climate Change 1995: The Science of Climate Change; Houghton, J. T.; Deng, Y.; Griggs, D. J.; Noguer, M.; von der Linden, P. J.; Dai, X.; Maskell, K.; Johnson, C. A. (Eds.); Cambridge University Press; Cambridge, UK, 1996.
6. Kärcher, B.; Peter, T.; Biermann, U. M.; Schumann, U. J Atmos Sci 1996, 53, 3066.
7. Minnis, P.; Young, D. F.; Garber, D. M. Geophys Res Lett 1998, 25, 1157–1160.
8. Strom, J.; Ohlsson, S. J Geophys Res 1997, 102, 23363.
9. Bockhorn, H. Soot Formation in Combustion: Mechanism and Models; Springer: Berlin, 1994.
10. Akhter, M. S.; Chughtai, A. R.; Smith, D. M. Appl Spectrosc 1985, 39, 143–153.
11. Akhter, M. S.; Chughtai, A. R.; Smith, D. M. Appl Spectrosc 1985, 39, 154–166.
12. Chughtai, A. R.; Gordon, S. A.; Smith, D. W. Carbon 1994, 32, 405–416.
13. Bidleman, T. F.; Foreman, W. T. In Advances in Chemistry 216; Hites, R. A.; Eisenreich, S. J. (Eds.); American Chemical Society: Washington, DC, 1987; pp. 27–56.
14. Haefliger, O. P.; Bucheli, T. D.; Zenobi, R. Analysis 1999, 27, 337–340.
15. Siegmann, K.; Sattler, K. J Chem Phys 2000, 112, 698–709.
16. Skillas, G.; Burtscher, H.; Siegmann, K.; Baltensperger, U. J Colloid and Interface Sci 1999, 217, 269–274.
17. Pires, M.; van den Bergh, H.; Rossi, M. J. J Atmos Chem 1996, 25, 229–250.
18. Stephens, S.; Rossi, M. J.; Golden, D. M. Int J Chem Kinet 1986, 18, 1133–1149.
19. Gao, R. S.; Kärcher, B.; Keim, E. R.; Fahey, D. W. Geophys Res Lett 1998, 25, 3323–3326.
20. Jacob, D. J Atmos Environ 2000, 34, 2131–2159.
21. Disselkamp, R. S.; Carpenter, M. A.; Cowin, J. P.; Berkowitz, C. M.; Chapman, E. G.; Zaveri, R. A.; Laulainen, N. S. J Geophys Res 2000, 105, 9767–9771.
22. Longfellow, C. A.; Ravishankara, A. R.; Hanson, D. R. J Geophys Res 2000, 105, 24345–24350.
23. Rogaski, C. A.; Golden, D. M.; Williams, L. R. Geophys Res Lett 1997, 24, 381–384.
24. Leu, M. T.; Choi, W. J Phys Chem 1998, 102, 7618–7630.
25. Kirchner, U.; Scheer, V.; Vogt, R. J Phys Chem 2000, 104, 8908–8915.
26. Saathoff, H.; Naumann, K. H.; Riemer, N.; Kamm, S.; Möhler, O.; Schurath, U.; Vogel, H.; Vogel, B. Geophys Res Lett 2001, 28, 1957–1960.
27. Jacquot, F.; Logie, V.; Brilhac, J. F.; Gilot, P. Carbon 2002, 40, 335–343.

28. Dorai, R.; Hassouni, K.; Kushner, M. J. J Appl Phys 2000, 88, 6060–6071.
29. Sakamaki, F.; Hatakeyama, S.; Akimoto, H. Int J Chem Kin 1983, 15, 1013.
30. Tabor, K.; Gutzwiller, L.; Rossi, M. J. J Phys Chem 1994, 98, 6172–6186.
31. Longfellow, C. A.; Ravishankara, A. R.; Hanson, D. R. J Geophys Res 1999, 104, 13833–13840.
32. Kalberer, M.; Ammann, M.; Arens, F.; Gäggeler, H. W.; Baltensperger, U. J. Geophys Res Atm 1999, 104, 13825–13832.
33. Stadler, D.; Rossi, M. J Phys Chem Chem Phys 2000, 2, 5420–5429.
34. Alcala-Jornod, C.; van den Bergh, H.; Rossi, M. J Phys Chem Chem Phys 2000, 2, 5584–5593.
35. Al-Abadleh, H. A.; Grassian, V. H. J Phys Chem 2000, 104, 11926–11933.
36. Barney, W. S.; Finlayson-Pitts, B. J. J Phys Chem A 2000, 104, 171–175.
37. Arens, F.; Gutzwiller, L.; Baltensperger, U.; Gäggeler, H. W.; Ammann, M. Environ Sci Technol 2001, 35, 2191–2199.
38. Kleffmann, J.; Becker, K. H.; Lackhoff, M.; Wiesen, P. Phys Chem Chem Phys 1999, 1, 5443–5450.
39. Ammann, M.; Kalberer, M.; Jost, D. T.; Tobler, L.; Rössler, E.; Piguet, D.; Gäggeler, H. W.; Baltensperger, U. Nature 1998, 395, 157–160.
40. Gerecke, A.; Thielmann, A.; Gutzwiller, L.; Rossi, M. J. Geophys Res Lett 1998, 25, 2453–2456.
41. Gao, R. S.; Kärcher, B.; Keim, E. R.; Fahey, D. W. Geophys Res Lett 1998, 25, 3323–3326.
42. Kotamarthi, V. R.; Gaffney, J. S.; Marley, N. A.; Doskey, P. V. Atmos Environ 2001, 35, 4489–4449.
43. Grassian, V. H. J Phys Chem A 2002, 106, 860–877.
44. Hauglustaine, D. A.; Ridley, B. A.; Solomon, S.; Hess, P. G.; Madronich, S. Geophys Res Lett 1996, 23, 2609–2612.
45. Kerminen, V. M.; Mäkeläa, T. E.; Ojanen, C. H.; Hillamo, R. E.; Vilhunen, J. K.; Rantanen, A. B.; Havers, N.; Von Bohlen, A.; Klockow, D. Environ Sci Technol 1997, 41, 1883–1889.
46. Weast, R. C. (Ed.); Handbook of Chemistry and Physics, 70th ed.; The Chemical Rubber Corporation; CRC Press: Boca Raton, FL, 1989–1990.
47. Caloz, F.; Fenter, F. F.; Tabor, K. D.; Rossi, M. J Rev Sci Instrum 1997, 68, 3172–3179.
48. Keyser, L.; Moore, S. B.; Leu, M.-L. J Phys Chem 1991, 95, 5496–5502.
49. Zabetakis, M. J. Flammability Characteristics of Combustible Gases and Vapors, Bulletin 627, Bureau of Mines, US Department of the Interior, 1965.